Supporting Information

Intercalation pseudocapacitance in 2D N-Doped V_2O_3 Nanosheets for stable and ultrafast Lithium-ion storage

Shiyu Yang[1], Ruizi Li*[1], Zhentao Nie[1], Hongjian Zhang[1], Yu Zhang[2], and Jixin Zhu[3]

[1] Frontiers Science Center for Flexible Electronics (FSCFE) & Institute of Flexible Electronics (IFE), Northwestern Polytechnical University, 127 West Youyi Road, Xi'an 710072, P. R. China

[2] School of Mechanical and Power Engineering, East China University of Science and Technology, Shanghai 200237, People's Republic of China

[3] State Key Laboratory of Fire Science, University of Science and Technology of China, 443 Huangshan Road, Hefei, 230027, P. R. China

Correspondence should be addressed to Ruizi Li; iamrzli@nwpu.edu.cn

Table of contents

1. Chemicals and Reagents S2
2. Structure characterization..S3
3. Electrochemical performance...S9
4. Lithium storage mechanism S18
Reference...S19

1. Chemicals and Reagents

Table S1 represents the reagents used in the experimental process. All the chemicals and reagents were used without further treatment.

Table S1 Chemicals and Reagents

Chemicals and Reagents	Chemical formula	Manufacturer	Product leverl
melamine	$C_3N_6H_6$	Aladdin	AR（>99%）
ultra-pure water	H_2O	Sinopharm	>99.5%
Vanadium pentoxide	V_2O_5	Aladdin	AR（>99%）
Hydrogen peroxide	H_2O_2	Aladdin	AR（30 wt%）
Copper foil	Cu		
lithium metal foil	Li		16*0.6mm
Anhydrous elthanol	C_2H_6O	Aladdin	AR（>99.9%）
polyvinylidene fluoride	PVDF		
Conductive agent	Super P		
N-methyl pyrrolidone	C_5H_9NO		
electrolyte	1 M LiPF6	Sinopharm	ethylene carbonate /dimethyl carbonate /ethyl methyl carbonate (1:1:1 in volume)

2. Structure characterization

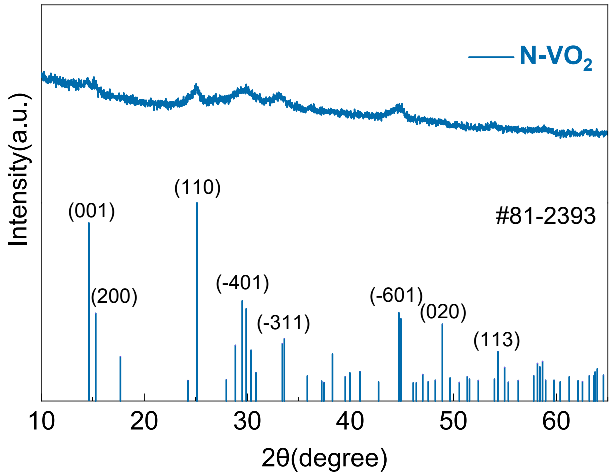

Figure S1 XRD pattern of N-VO_2 sample.

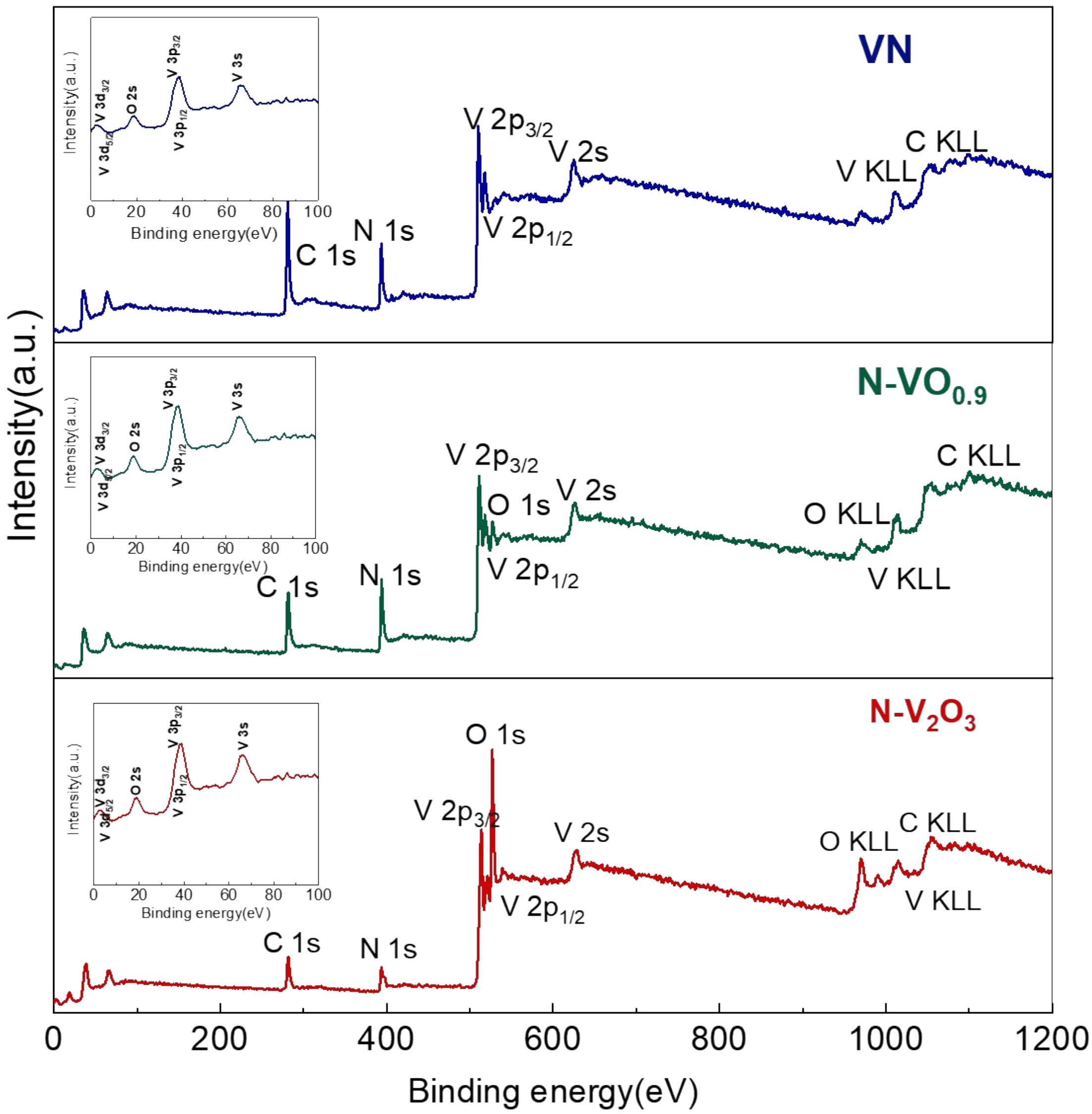

Figure S2. XPS of N-V_2O_3, N-$VO_{0.9}$ and VN samples.

Table S2. Elemental analysis results for N-V_2O_3 samples

Sample	V (wt %)	N (wt %)	O (wt %)
N-V_2O_3	93.6	4.6	1.8

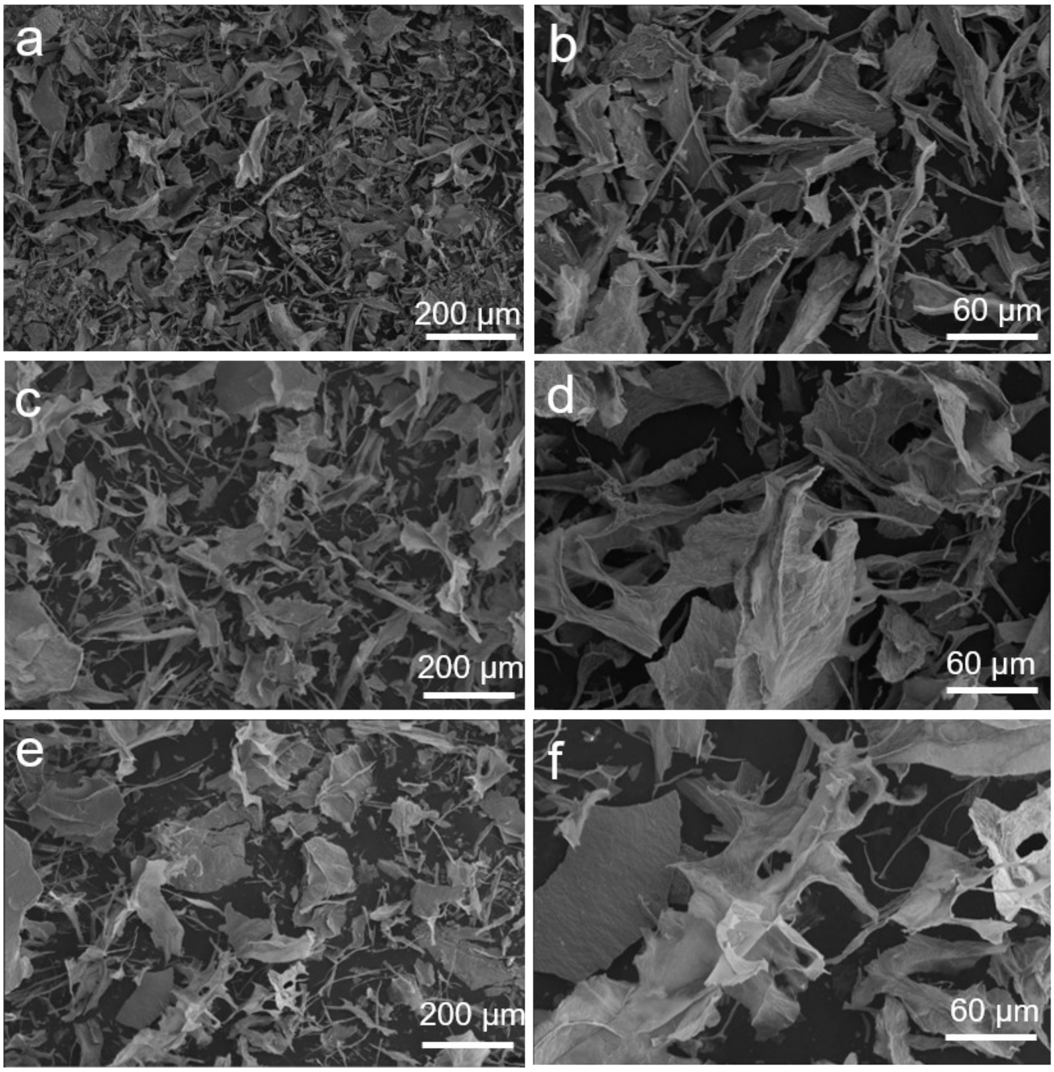

Figure S3. (a-b), (c-d) and (e-f) SEM images of the samples synthesized for N-V_2O_3, N-$VO_{0.9}$ and VN samples at low magnification and medium magnification, respectively.

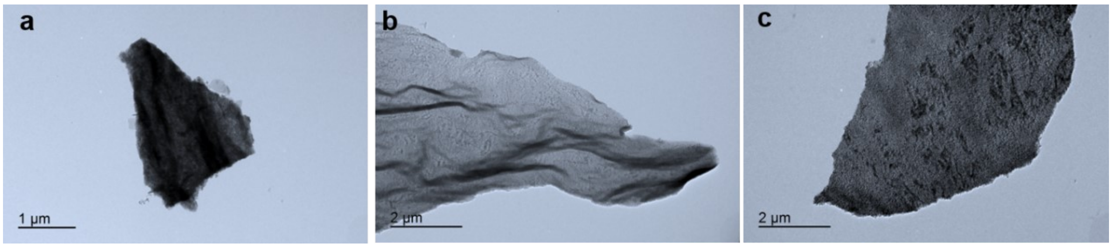

Figure S4. (a-c) TEM images of the obtained N-V_2O_3, N-$VO_{0.9}$ and VN samples at low magnification, respectively.

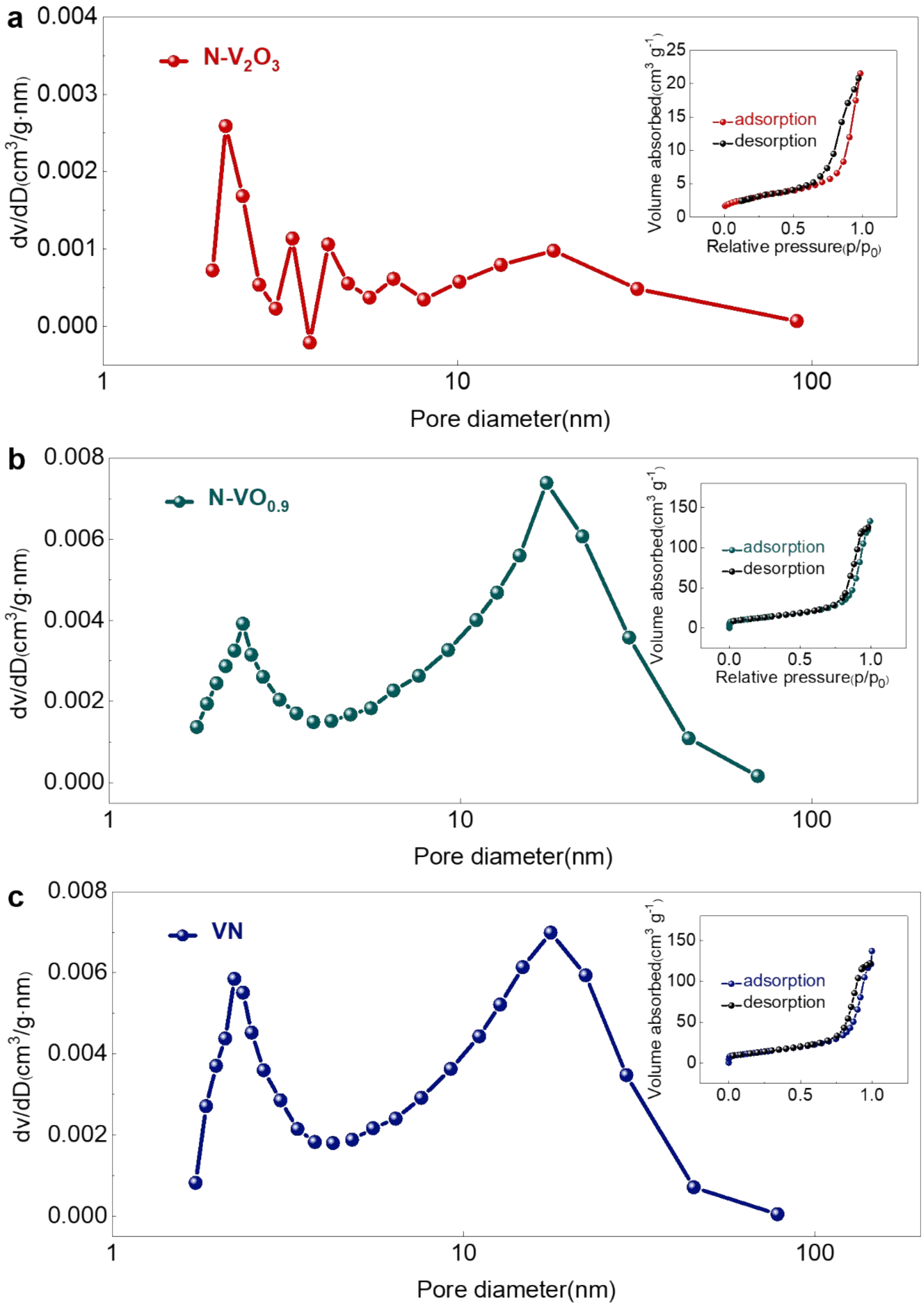

Figure S5. Pore size distribution curve (calculated based on Barrett-Joyner-Halenda (BJH) method) and nitrogen adsorption-desorption isotherm (insert) of (a) N-V_2O_3, (b) N-$VO_{0.9}$ and (c) VN samples.

3. Electrochemical performance

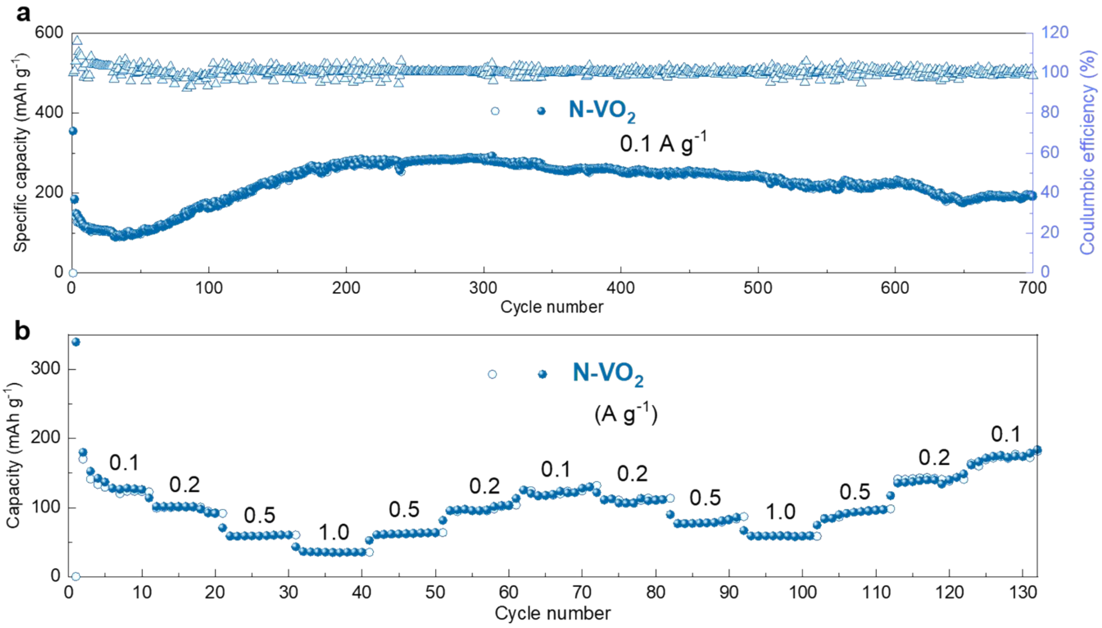

Figure S6 (a) Cycling performances of N-VO_2 electrode at 0.1 A g^{-1}. (b) Rate capabilities of N-VO_2 electrode at different current densities.

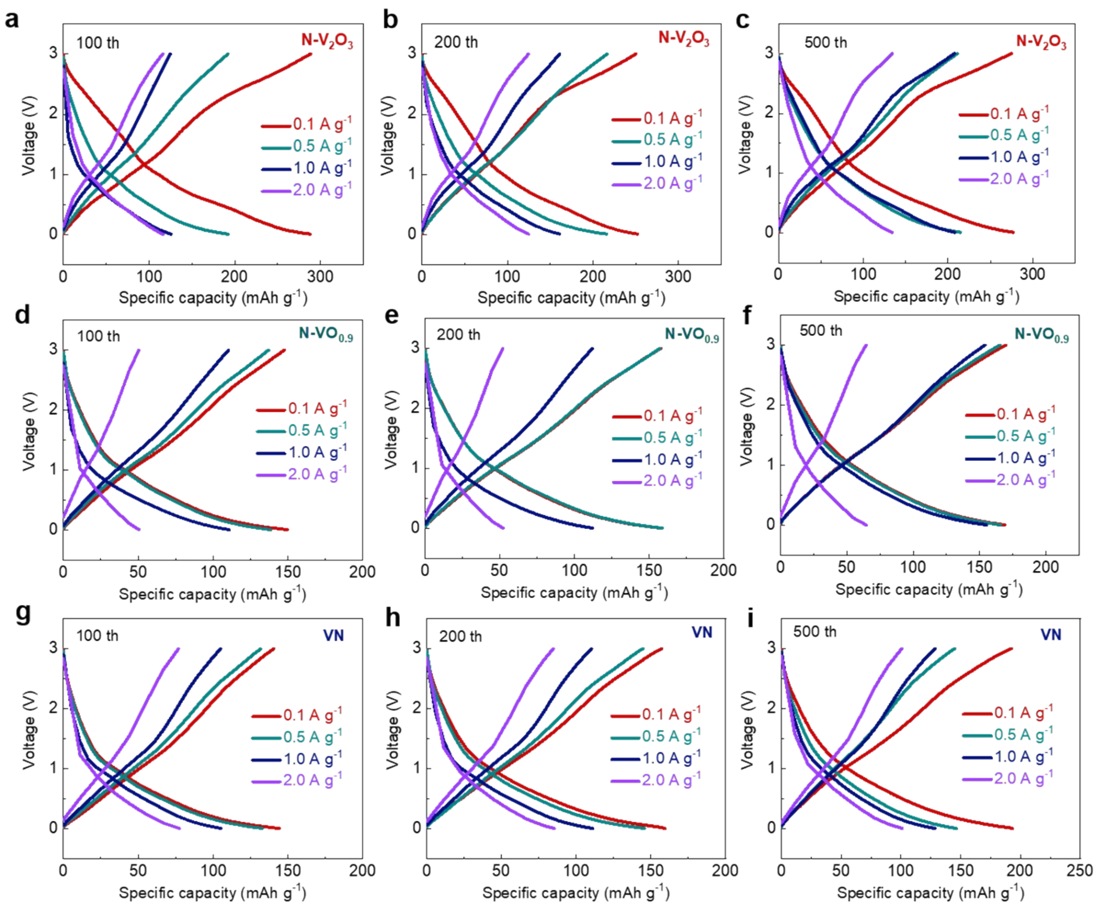

Figure S7. Charge-discharge curves of (a-c) N-V_2O_3, (d-f) N-$VO_{0.9}$ and (g-i) VN electrodes at 0.1, 0.5, 1.0 and 2.0 A g^{-1}, respectively.

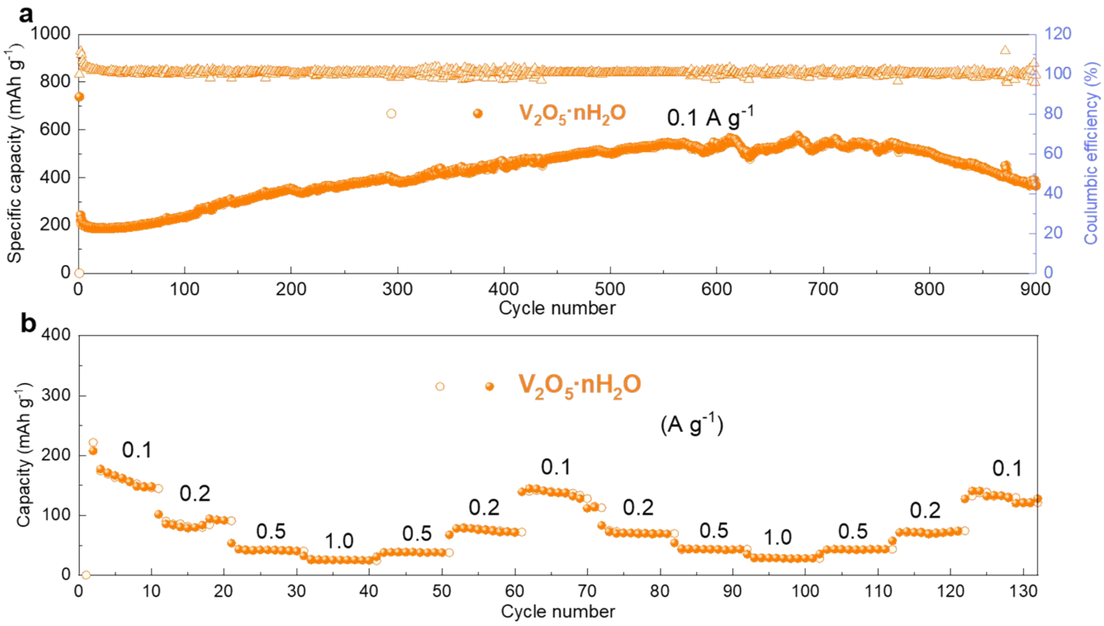

Figure S8. (a) Cycling performances of $V_2O_5 \cdot nH_2O$ electrode at 0.1 A g^{-1}. (b) Rate capabilities of $V_2O_5 \cdot nH_2O$ electrode at different current densities.

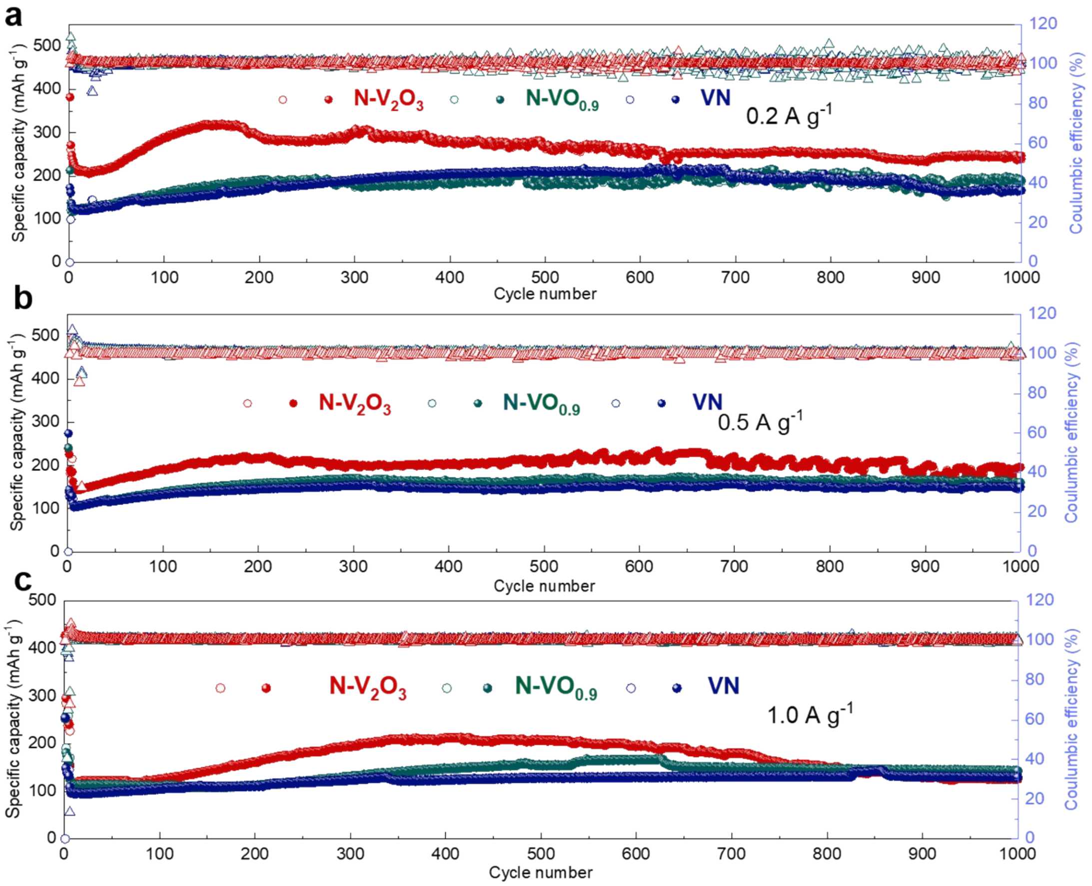

Figure S9. Cycling performances of N-V_2O_3, N-$VO_{0.9}$ and VN electrodes at (a) 0.2 A g^{-1}, (b) 0.5 A g^{-1} and (c) 1.0 A g^{-1}, respectively.

Table S3 Electrochemical performance comparison of the as-prepared N-V_2O_3 with other reported V_2O_3-based anode materials for Li-ion batteries.

Materials	Capacity (mAh g^{-1} / A g^{-1})	Rate capability (mAh g^{-1} / A g^{-1})	Cycling stability (mAh g^{-1} / cycles / A g^{-1})	Reference
Co-V_2O_3	477.1/0.1	467.6/0.2 470/1.0 444.4/0.5	986.2/630/0.5	[1]
V_2O_3@C	179.1/0.1	179.1/0.1 162.6/0.2 107.4/1.0	—	[2]
multi-shelled V_2O_3/C	216/0.1	216/0.1 205/0.2 176/1.0	173/2000/10	[3]
C@V_2O_3	300/0.1	215/0.5	120/500/0.1	[4]
V_2O_3@NC	523/0.1	523/0.1 487/0.5 384/1.0	317/1000/2.0	[5]
N-V_2O_3	348/0.1	348/0.1 319/0.2 260/0.5	346/1000/0.1	This work

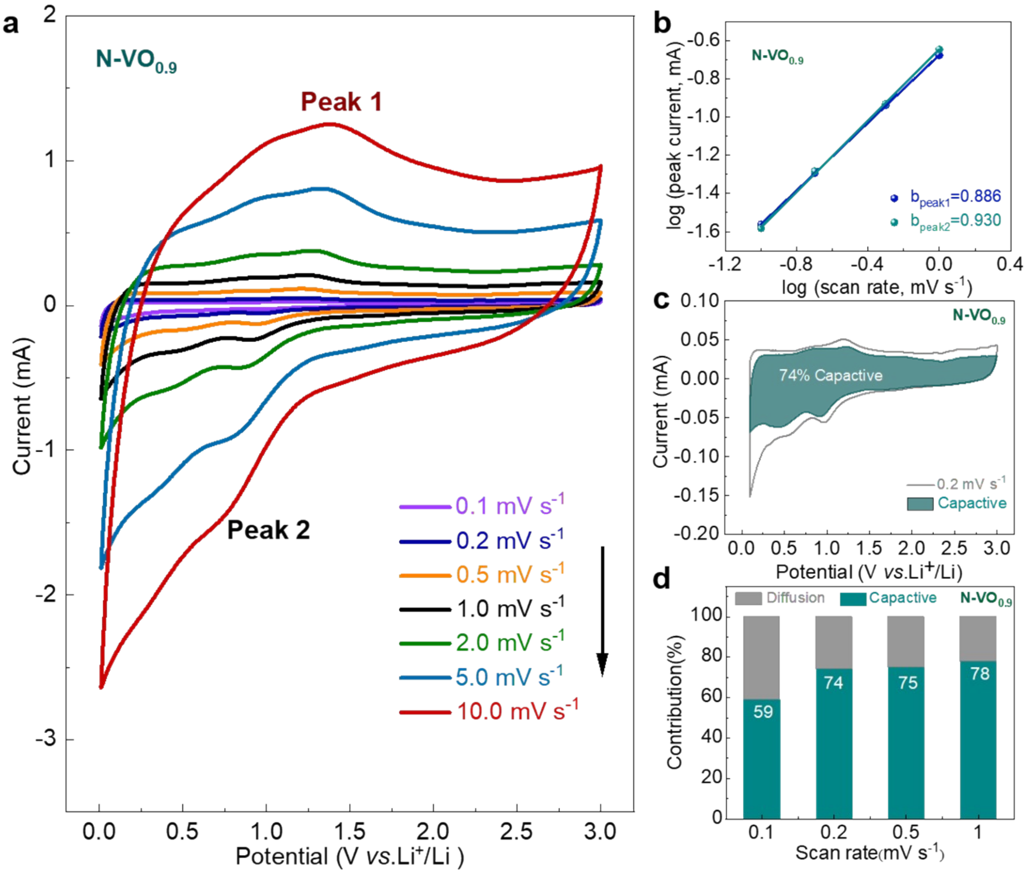

Figure S10. (a) CV curves of N-$VO_{0.9}$ electrode at various scan rates from 0.1 to 10 mV s^{-1} within a potential range of 0.01 to 3.00 V (vs. Li^+/Li). (b) Fitted lines and log (peak current) vs.log (scan rate) plot of N-$VO_{0.9}$ electrode at various oxidation and reduction states. (c) Capacitive contribution of N-$VO_{0.9}$ electrode shown by the shaded region at 0.2 mV s^{-1}. (d) Capacity contribution of N-$VO_{0.9}$ electrode at various scan rates.

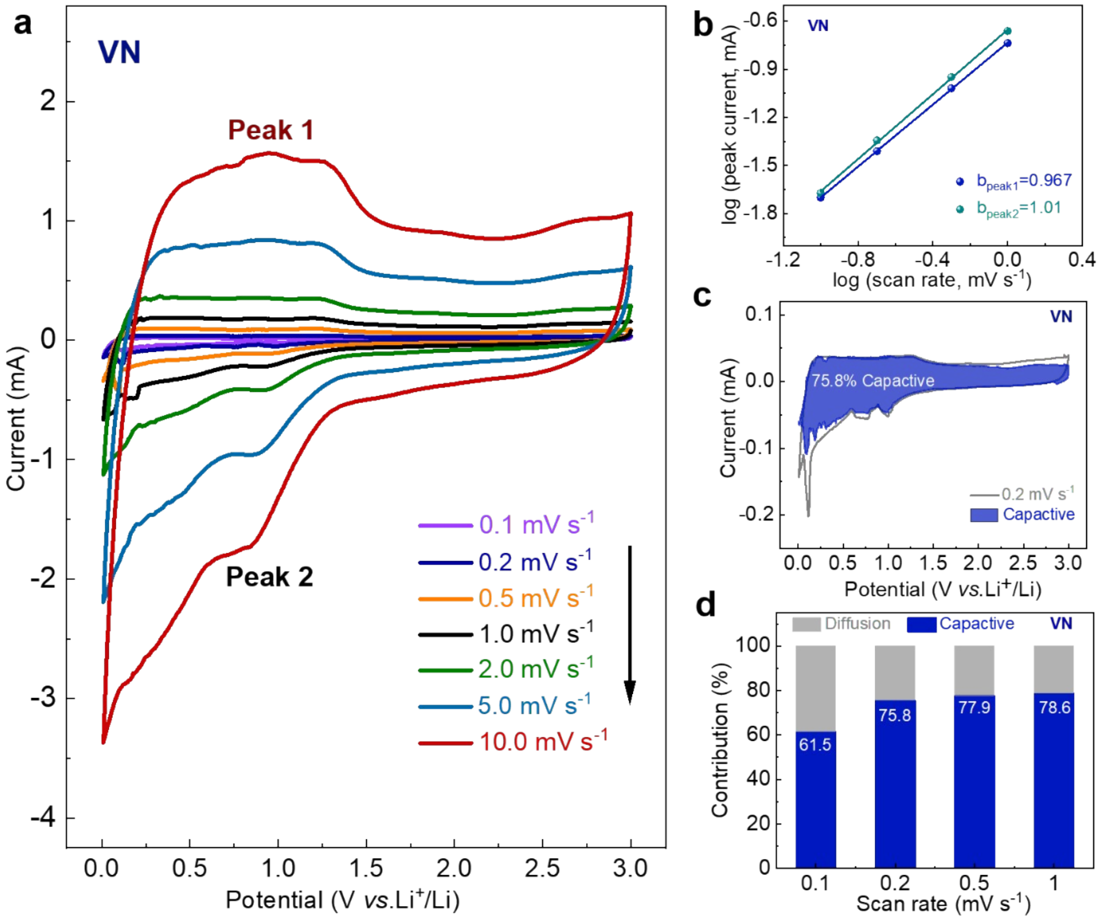

Figure S11. (a) CV curves of VN electrode at various scan rates from 0.1 to 10 mV s^{-1} within a potential range of 0.01 to 3.00 (V vs. Li^+/Li). (b) Fitted lines and log (peak current) vs.log (scan rate) plot of VN electrode at various oxidation and reduction states. (c) Capacitive contribution of VN electrode shown by the shaded region at 0.2 mV s^{-1}. (d) Capacity contribution of VN electrode at various scan rates.

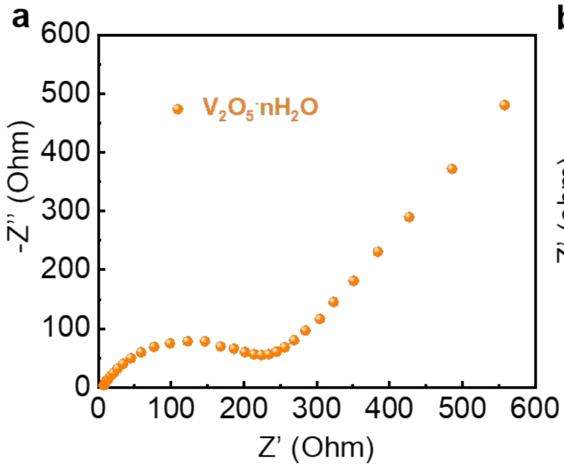

Figure S12. (a) Electrochemical impedance spectroscopy of $V_2O_5{\cdot}nH_2O$ electrode. (b) Fitted curves by Z′ and $\omega^{-1/2}$ of $V_2O_5{\cdot}nH_2O$ electrode.

The Li^+ diffusion coefficient of can be calculated: [6-7]

$$Z' = R_0 + R_{ct} + \sigma\omega^{-\frac{1}{2}} \quad \text{S1}$$

$$D_{Li^+} = \frac{R^2T^2}{2A^2n^4F^4C^2\delta^2} \quad \text{S2}$$

where R, T, A, n, F, C and σ stand for gas constant, Kelvin temperature, the surface of the electrode, the number of electrodes each molecule during reaction, Faraday constant, the concentration of Li^+, the Warburg factor, respectively. Thus, if it guarantees other same parameters, the D_{Li+} of N-V_2O_3 electrode is far higher than N-$VO_{0.9}$, and VN electrodes.

4. Lithium storage mechanism

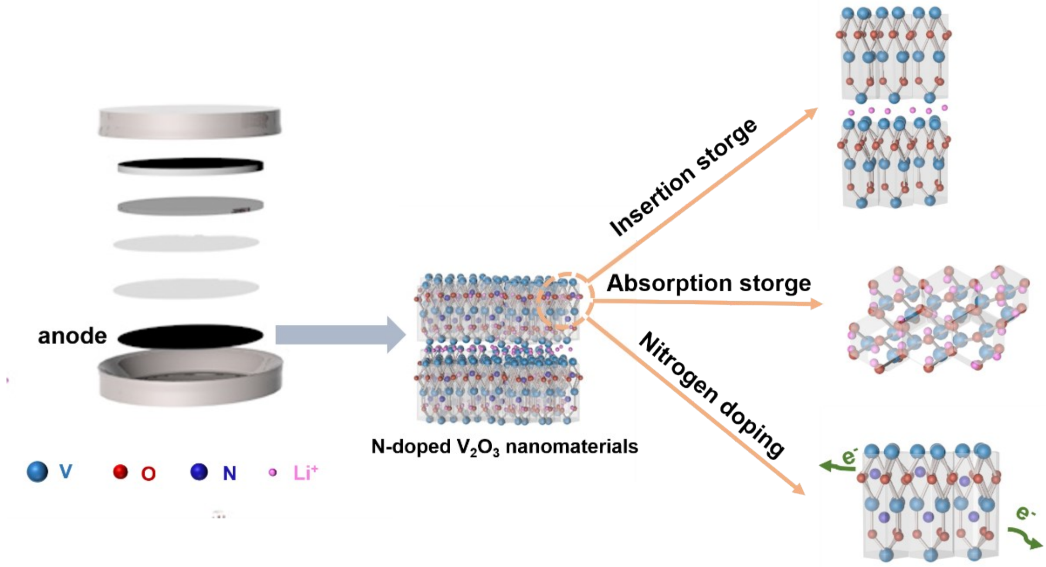

Figure S13. Schematic illustration of Li^+ storage mechanism in the N-V_2O_3 electrode.

Reference

[1] S. Zhang, L. Zhang, G. C. Xu, X. L. Zhang and A. H. Zhao, Synthesis of cobalt-doped V_2O_3 with a hierarchical yolk–shell structure for high performance lithium-ion batteries, *CrystEngComm*, 2020, **22**,1705–1711.

[2] W. Q. Xu, Y. Niu, D. H. Wang, H. M. Li, S. Y. Zhang, S. M. Zeng, L. D. Li, Y. J. Ma, L. J. Zhi and X. L. Li, Scalable fabrication of carbon-networked size-tunable V_2O_3 for lithium storage, *ACS Appl. Energy Mater.*, 2022, **5**, 3757-3765.

[3] Y. T. Li, S. Zhang, S. T. Wang, J. Leng, C. H. Jiang, X. W. Ren, Z. T. Zhang, Y. Yang and Z. L. Tang, A multi-shelled V_2O_3/C composite with an overall coupled carbon scaffold enabling ultrafast and stable lithium/sodium storage, *J. Mater. Chem. A.*, 2019, **7**, 19234-19240.

[4] D. N. Lei, H. Ye, C. Liu, D. C. An, J. M. Ma, W. Lv, B. H. Li, F. Y. Kang, and Y. B. He, Interconnected ultrasmall V_2O_3 and $Li_4Ti_5O_{12}$ particles construct robust interfaces for long-cycling anodes of lithium-ion batteries, *ACS Appl. Mater. Interfaces*, 2019, **11**, 29993−30000.

[5] X. F. Zhang, L. C. Xun, S. Gao, Y. M. Xu, X. L. Cheng, H. Zhao and L. H. Huo, Facile synthesis of V_2O_3@N-doped carbon nanosheet arrays on nickel foam as free-standing electrode for high performance lithium ion batteries, *Catal. Today.,* 2021, **374**, 117-123.

[6] M. Wu, K. J. Zhu, P. H. Liang, Z. R. Yao, F. Shi, J. Zhang, K. Yan, J. S. Liu and J. Wang, Uniform rotate hydrothermal synthesis of V_6O_{13} nanosheets as cathode material for lithium-ion battery, *Journal of Alloys and Compounds*, 2021, **877**,

160174.

[7] X. F. Zhang, L. C. Xun, S. Gao, Y. M. Xu, X. L. Cheng, H. Zhao, L. H. Huo. Facile synthesis of V_2O_3@N-doped carbon nanosheet arrays on nickel foam as free-standing electrode for high performance lithium ion batteries, *Catalysis Today*, 2021**,** **374**, 117-123.